

# Quantum simulation of non-trivial topology

Octavi Boada

*Physics of Information Group, Instituto de Telecomunicações, P-1049-001 Lisbon, Portugal*

Alessio Celi and Maciej Lewenstein

*ICFO-Institut de Ciències Fotòniques, Barcelona, Spain*

Javier Rodríguez-Laguna

*IFT-Instituto de Física Teórica, UAM-CSIC, Madrid, Spain and*

*ICFO-Institut de Ciències Fotòniques, Barcelona, Spain*

José I. Latorre

*Dept. ECM, Universitat de Barcelona, Spain*

We propose several designs to simulate quantum many-body systems in manifolds with a non-trivial topology. The key idea is to create a synthetic lattice combining real-space and internal degrees of freedom via a suitable use of induced hoppings. The simplest example is the conversion of an open spin-ladder into a closed spin-chain with arbitrary boundary conditions. Further exploitation of the idea leads to the conversion of open chains with internal degrees of freedom into artificial tori and Möbius strips of different kinds. We show that in synthetic lattices the Hubbard model on sharp and scalable manifolds with non-Euclidean topologies may be realized. We provide a few examples of the effect that a change of topology can have on quantum systems amenable to simulation, both at the single-particle and at the many-body level.

## I. INTRODUCTION

The research field of quantum simulation explores, among other goals, the possibility of using well-controlled quantum systems to simulate the behavior of other quantum systems whose dynamics escapes standard theoretical or experimental approaches. As a relevant example, quantum simulators have been used to successfully analyse condensed matter phenomena [1]. Through synthetic gauge fields [2], more ambitious and multidisciplinary problems can be addressed, such as the determination of the phase diagram of (lattice) gauge theories [3–8]. This theoretical progress is supported by vigorous experimental developments with a growing number of platforms available for quantum simulation like cold neutral atoms and molecules [9], trapped ions [10], photonic crystals [11], NV-centers [12], and superconducting qubits [13].

On a different line of research, topological models have attracted great interest as well. Topology is a key feature to understand many physical phenomena, such as the quantum Hall and quantum spin-Hall effects [14], quantization of Dirac monopole charge [15], charge fractionalization and non-perturbative properties of vacua of Yang-Mills theories [16–19], etc. Topology also plays an essential role in engineering novel states of ultracold matter, such as topological insulators [20]. Notably, topological protection has been considered as a resource for quantum computation [21]. Nonetheless, non-trivial topology is not easy to implement in practical systems. For instance, there is no obvious way to manipulate a 2D condensed matter system to be topologically connected as on a higher genus Riemann surface. Experimental

limitations are thus an obstacle to analyse the effects of non-trivial topologies on quantum systems.

The reunion of these two topics, namely quantum simulation and topology, is a natural and tantalizing evolution for both sets of ideas. So far, the focus in quantum simulation has been on topological properties emerging in infinite systems due to their dynamics, e.g., in the toric code [22–24] or in periodically driven systems [25–27], and in synthetic quantum Hall [28–31] and quantum spin-Hall [32–36] systems that exhibit edge states when subjected to open boundary conditions. The search for edge states includes also theoretical and experimental efforts in understanding Majorana fermions, since they are produced at the boundaries of some quantum systems [37–39]. But, so far, the simulation of systems with non-trivial boundary conditions, with the exception of circle/torus geometry (cf. theory [40–42], and experiments [43–49], and references therein), has been very scantily explored (see also [50, 51], which appeared while this work was in progress).

Geometry and topology have already made their appearance in quantum simulators, specifically in optical lattices with ultracold atoms. Recently, there have been proposals to simulate quantum many-body physics in certain types of curved background spacetimes [52], tailoring the hopping amplitudes of the optical lattice. Moreover, in [53] a protocol was introduced to use the different atomic states as an artificial extra dimension. This latter proposal plays a key role in our approach to the simulation of quantum matter in different topologies. In effect, by managing the internal interactions between the internal states, we will show how to turn an open 1D optical lattice into a system with periodic boundary conditions, a cylinder, a torus or a Möbius strip. Our proposal can

be engineered also using other platforms and/or may be combined with other techniques such as the ones allowing for well-established toroidal compactifications [54–69], or the speckle potentials allowing to simulate in a controlled way disorder [70, 71].

The paper is organized as follows. Section II presents the general strategy to simulate non-trivial topology on a quantum system, while the experimental aspects are discussed in section III. Section IV is devoted to an analysis of signatures of non-trivial topological effects, which can be observed in systems amenable to experimental realization. We end up, in section V presenting the conclusions and a discussion of the possibilities for future work.

## II. ARTIFICIAL TOPOLOGY

The general aim of our work is to build quantum simulators for dynamics in different topologies out of an optical lattice, which naturally have open boundary conditions. In order to illustrate our strategy let us start with the simplest paradigmatic example: simulating quantum dynamics on a ring i.e., a 1D system with periodic boundary conditions (PBC). In principle, this can be achieved by embedding it into a plane, bending it into a circumference and creating an effective interaction between the two extremes which is identical to the one in the bulk. Thus, an extra dimension is required, as well as the possibility of bending the system without altering its dynamical properties. Both requirements are difficult to meet. Therefore, we shall explore a different possibility, which amounts to engineering an artificial extra dimension.

For definiteness, let us discuss a bosonic 1D hopping model with  $L$  sites whose Hamiltonian is merely kinetic. Let  $a_i^\dagger$  create a boson at site  $i$ . The PBC are obtained by connecting the end points with an extra term.

$$H_c = - \left( J \sum_{i=1}^{L-1} a_i^\dagger a_{i+1} + J_c a_1^\dagger a_L \right) + H.c., \quad (1)$$

where  $J_c$ , the closing hopping, should be taken as  $J_c = J$ . The problem of simulating an  $S^1$  topology is tantamount to generating this closing term which connects both boundaries of the system. There are several generic strategies to create that term:

- Embed the system in a plane and bend it until both boundaries touch, thus reducing the boundary term to an ordinary bulk term.
- Induce a long-range hopping through a medium or an intermediate state.
- Use a synthetic dimension.

This work focuses on the last solution. The introduction of an extra dimension through internal degrees of freedom was proposed in [53]. Indeed, an open 1D line

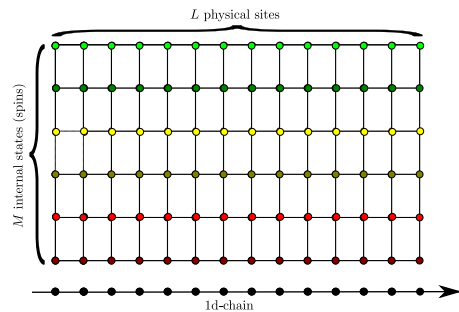


FIG. 1. Idea of a synthetic lattice: a 1D chain of length  $L$  sites with  $M$  species is equivalent to a  $L \times M$  synthetic lattice, once the chain is dressed with appropriate couplings between species.

of  $L$  sites, each endowed with  $M$  internal states, can be regarded as an  $L \times M$  synthetic 2D lattice, see Fig. 1. In geometric terms, we can think of the internal states as a fiber opening at each real-space site. The resulting synthetic lattice would be, therefore, a discrete analogue of a fibre bundle. A generic hopping Hamiltonian for this system can be written as

$$H = - \left( \sum_{\sigma, \sigma'} \sum_{i=1}^{L-1} J_{i, \sigma, \sigma'}^v b_i^{\dagger(\sigma)} b_i^{(\sigma')} + J_{i, \sigma, \sigma'}^h b_i^{\dagger(\sigma)} b_{i+1}^{(\sigma')} \right) + H.c., \quad (2)$$

where  $J^v$  and  $J^h$  are sets of vertical and horizontal hoppings, in the synthetic lattice view. The vertical term allows us to connect any pair of internal states in the same physical site, while the horizontal term allows us to connect any two internal states in physically neighboring sites.

Figure 2 illustrates the process by which we can convert an open spin chain with  $M = 2$  states per site into a system with PBC. In Eq. (2), simply set  $J_{i, \sigma, \sigma'}^h = J \delta_{\sigma, \sigma'}$  and  $J_{i, \sigma, \sigma'}^v$  to be zero in the bulk, but not in the extremes,  $i = 1$  or  $i = L$ , in which case we have a connecting term between the two species:  $J_{i, 1, 2}^v = J$ . If we introduce  $2L$  virtual particle creation operators,  $a_j = b_j^{(1)}$  and  $a_{2L+1-j} = b_j^{(2)}$ ,  $j = 1, \dots, L$ , the Hamiltonian reads exactly as a 1D-PBC hopping Hamiltonian.

Let us summarize the idea. By inducing appropriate hoppings on the internal degrees of freedom —whether we call them species, spin values, etc.— we can attain effectively higher-dimensional dynamics, giving them a geometric meaning [53]. This higher dimension can be bent and sewn in different ways, as shown in the previous example. The simplest application consists on turning an open chain with two species into a closed one with a single species. It only needs localized control of the transformations between the species at the boundaries of the open system.

As an additional feature, our synthetic approach allows to control the phases of the induced hoppings. This

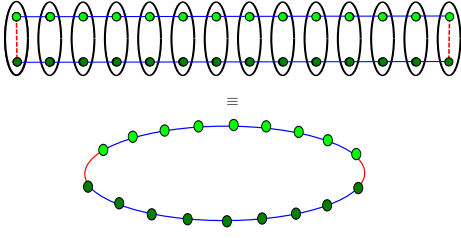


FIG. 2. Engineering a circumference of  $2L$  lattice sites from a  $L$  synthetic lattice that carries  $M = 2$  species. The blue solid links indicate the hopping along the chain, e.g., the free hopping in a cold-atom implementation, while the two dashed red links are induced local interactions between the two species, e.g., a Raman coupling between hyperfine levels of atoms. The vertical black ellipses represent the physical sites in the real 1D-chain occupied by the two species.

is equivalent to inducing a magnetic field piercing the chain and, via a gauge transformation, to create boundary conditions which interpolate continuously between periodic and anti-periodic ones. In critical 1D spin models a non-trivial magnetic flux can be regarded as a defect in the associated conformal field theory (CFT) [72, 73].

The 1D-PBC lattice described above is the basic building block for more interesting 2D models. In the next sections we will discuss more exotic boundary conditions, such as Möbius strips.

### A. Assembling cylinder and torus

A cylinder can be understood as a fiber bundle of segments emerging from each point of a circumference. Let us describe how to create cylindrical synthetic lattice (i.e., a ladder with PBC) of size  $2L_x \times L_y$  from a 1D open chain of  $L_x$  real sites, with  $M = 2L_y$  internal states per site. Let  $a_{i,j}^\dagger$  create a particle at site  $(i, j)$  of the cylinder. Its correspondent in the synthetic lattice will be  $b_i^{\dagger(2j-1)}$  if  $i \leq L_x$  and  $b_{2L_x+1-i}^{\dagger(2j)}$  otherwise. An example with  $L_y = 2$  is shown in figure 3.

The Hamiltonian of a free bosonic system on a cylinder can be written as

$$H = -J \left( \sum_{i=1}^{2L_x} \sum_{j=1}^{L_y} a_{i,j}^\dagger (a_{i+1,j} + a_{i,j+1}) + \sum_{j=1}^{L_y} a_{2L_x,j}^\dagger a_{1,j} \right) + H.c. \quad (3)$$

which can be mapped to the form (2). If  $i \neq 1$  and  $i \neq L$ , we have

$$\begin{aligned} J_{i,\sigma,\sigma'}^h &= J \delta_{\sigma,\sigma'} \\ J_{i,\sigma,\sigma'}^v &= J B_{\sigma,\sigma'} \end{aligned} \quad (4)$$

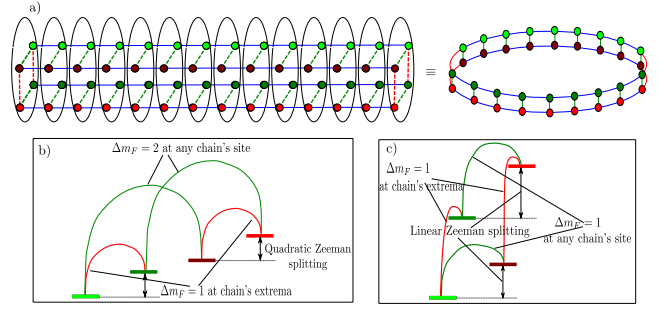


FIG. 3. Engineering a cylinder of basis  $L_x$  and height  $L_y$  lattice sites from a  $L \times M$  synthetic lattice with  $L = L_x/2$  and  $M = 2L_y$ . (a)  $L_y = 2$  synthetic cylinder. In a cold atom implementation, the blue solid links indicate the free hopping while the dashed ones are laser or radio-frequency induced. The dashed red links are the “sewing” hoppings  $C_{\sigma\sigma'}$  closing each circle of the cylinder, while the dashed green ones are the hoppings  $B_{\sigma\sigma'}$  along its height, connecting the different circles. (b) and (c) Spectroscopical arrangement of the four internal degrees of freedom in the one-manifold and two-manifold scheme, respectively. The former can be realized by using the groundstate of atoms  $F \geq \frac{3}{2}$  like Li, K, Yb, Sr, Er, etc, and requires quadratic Zeeman splitting in order to have  $J'$ -coupling (in red) only between odd-even  $m_F$ -states. The latter requires earth-alkali like atoms with  $F \geq \frac{1}{2}$  as  $^{171}\text{Yb}$ ,  $^{173}\text{Yb}$ , and  $^{87}\text{Sr}$  and in this case the linear splitting is sufficient in order to make the spin accessible by Raman lasers or radio-frequency pulses.

where  $B_{\sigma,\sigma'}$  is a  $2L_y \times 2L_y$  bulk Hermitian matrix of internal hoppings implementing motion in the transverse direction of the cylinder

$$B_{\sigma,\sigma'} = \delta_{\sigma,\sigma' \pm 2}, \quad (5)$$

i.e., it is always possible to jump between internal states differing by two units. On the extremes, for  $i = 1$  or  $i = L$ , we have to add a new term

$$J_{i,\sigma,\sigma'}^v = J B_{\sigma,\sigma'} + J C_{\sigma,\sigma'} \quad (6)$$

where  $C_{\sigma,\sigma'}$  is a closing Hermitian matrix which is responsible for sewing the open edges of the cylinder. Since it corresponds to a pile of circumferences, the non-zero entries of those matrix are of the form  $C_{2j-1,2j}$  and  $C_{2j,2j-1}$ . The geometrical meaning of that closing matrix is that each horizontal line bends on itself, without mixing.

The synthetic cylinder we just described can be easily turned into a torus by changing matrix  $B_{\sigma,\sigma'}$ , with the introduction of new non-zero terms  $B_{1,2L_y-1} = B_{2L_y-1,1} = B_{2,2L_y} = B_{2L_y,2} = 1$  which sew together the upper and lower ends of each fiber, see Fig. 4. This construction makes sense for  $L_y \geq 3$ . In other terms, each fiber becomes a circumference instead of an open segment. However, while the number of layers,  $L_y$ , of the cylinder are

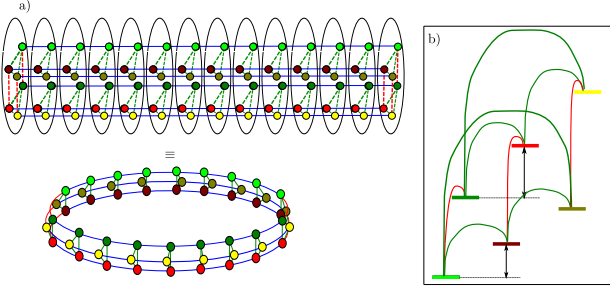


FIG. 4. Engineering a torus by converting each fiber into a circumference. In (a) we show the  $L_y = 3$  synthetic torus. In a cold atom implementation, the blue solid links indicate the free hopping while the dashed ones are laser or radio-frequency induced. The dashed red links are unchanged with respect to Fig. 3 (a), while additional green dashes ones are used to glue the basis of the cylinder connecting the top and bottom circles, and correspond to the additional terms in  $B_{\sigma\sigma'}$ . In (b) we show the spectroscopical arrangement of the six internal degrees of freedom in the two-manifold scheme requiring  $F \geq \frac{3}{2}$ , for instance,  $^{173}\text{Yb}$ .

limited only by the total number of internal species available, in the case of the torus  $L_y$  can be further restricted by the ability of coupling the internal species cyclically (see sect. III for cold atom implementation).

### B. Möbius strip and twisted torus

The analogy of the synthetic lattice and the fiber bundle, with the internal states playing the role of the fiber, can be exploited further. We can glue the fibers opening at different sites in a different way, in order to provide a non-trivial topology to the manifold. For example, by gluing the first and last fibers of a cylinder via a reflection we can turn it into a non-orientable manifold, a Möbius strip.

Let us discuss in detail the construction of the artificial Möbius strip, a  $2L_x \times L_y$  ladder with twisted boundary conditions, i.e., site  $(2L_x, j)$  is connected to site  $(1, L_y + 1 - j)$ . The free Hamiltonian reads

$$H = J \left( \sum_{i=1}^{2L_x-1} \sum_{j=1}^{L_y-1} a_{i,j}^\dagger (a_{i+1,j} + a_{i,j+1}) + \sum_{j=1}^{L_y-1} a_{2L_x,j}^\dagger a_{1,L_y+1-j} \right) + H.c. \quad (7)$$

The corresponding synthetic lattice Hamiltonian corresponds to the general form (2), with the following choice of hoppings, see Fig. 5. For sites  $i \neq 1$  and  $i \neq L$ , they are the same as for the cylinder, Eq. (4). For the extremes, one of them should be the same as for the cylinder, say  $i = L$ . But  $i = 1$  must be twisted and connect

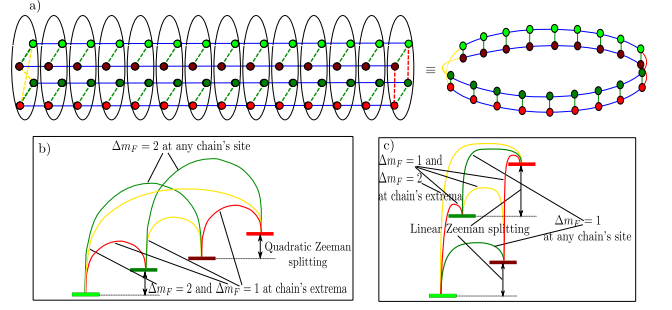


FIG. 5. Engineering a Möbius strip by twisting the cylinder. In (a) we show the  $L_y = 2$  synthetic strip. In a cold atom implementation, the blue solid links indicate the free hopping while the dashed ones are laser or radio-frequency induced. The dashed green links and half of the dashed red links are unchanged with respect to Fig. 3 (a), while the yellow dashed ones are the twisted closing hoppings connecting different circles, reflecting the change from  $C_{\sigma\sigma'}$  to  $C_{\sigma\sigma'}^M$ . In (b) and (c) we see the spectroscopical arrangement of the four internal degrees of freedom in the one-manifold and two-manifold scheme, respectively. The former can be realized by using the ground state of atoms  $F \geq \frac{3}{2}$  like Li, K, Yb, Sr, Er, etc., while the latter requires earth-alkali like atoms with  $F \geq \frac{1}{2}$  as  $^{171}\text{Yb}$ ,  $^{173}\text{Yb}$ , and  $^{87}\text{Sr}$ . In both cases, the hyperfine levels are linearly split in order to make them accessible by multiple Raman lasers or radio-frequency pulses.

the different values of the transverse coordinate

$$J_{1,\sigma,\sigma'}^v = J B_{\sigma,\sigma'} + J C_{\sigma,\sigma'}^M, \quad (8)$$

where  $B_{\sigma,\sigma'}$  is the bulk matrix, given by Eq. (5) and the Möbius closing matrix,  $C_{\sigma,\sigma'}^M$ , has non-zero terms which revert the site ordering of the extra dimension, i.e., connects sites  $y = j$  with  $y = L_y + 1 - j$ . Therefore, we get that the non-zero elements of  $C^M$  have the form  $C_{2j-1,2(L_y+1-j)}^M$  (and symmetric) and  $C_{2j,2(L_y+1-j)-1}^M$ . See the  $L_y = 2$  case exemplified in Fig. 5, where at site  $i = 1$  the (yellow) hoppings glue the two different circles.

Of course, this scheme presents the handicap that the size of the transverse direction is not scalable, i.e., it is limited by the number of internal species available and by our ability to couple them. But, as we will see in the next sections, already with  $L_y = 2$  we can obtain substantial differences between the cylinder and the Möbius strip.

We can combine the schemes for the Möbius strip and the torus in order to build a *twisted torus*. The real space Hamiltonian corresponds to (7) with the extra term connecting the  $y = 1$  and  $y = L_y$  values of all fibers:  $J \sum_{i=1}^{2L_x} a_{i,1}^\dagger a_{i,L_y} + H.c.$ . This maps into  $J \sum_{i=1}^{L_x} b_i^{\dagger(1)} b_i^{(2L_y-1)} + b_i^{\dagger(2L_y)} b_i^{(2)}$  for the synthetic lattice Hamiltonian. See Fig. 6 for an illustration.

More general boundary conditions, which do not correspond to a 2D manifold, are related to the application of a general unitary matrix of hoppings between sites at

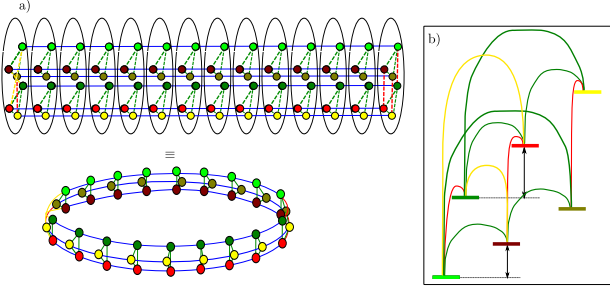


FIG. 6. Engineering a twisted torus by wrapping the Möbius strip. Equivalently, a twisted torus can be visualized as a torus cut and glued with a twist. In (a) we see the  $L_y = 3$  synthetic twisted torus. In a cold atom implementation, the blue solid links indicate the free hopping while the dashed ones are laser or radio-frequency induced. The dashed red links are unchanged with respect to Fig. 5 (a), while the green dashed ones are used to glue the borders of the Möbius strip. In (b) we show the spectroscopical arrangement of the six internal degrees of freedom in the two-manifold scheme, which requires  $F \geq \frac{3}{2}$  as, for instance, in  $^{173}\text{Yb}$ .

$i = 2L_x$  and  $i = 1$ , which can be parametrized as

$$\sum_{j,j'=1}^{L_y} U_{j,j'} a_{2L_x,j}^\dagger a_{1,j'} + H.c. \quad (9)$$

where  $U \in \text{U}(L_y)$ . If  $U$  is the identity matrix, we obtain the cylinder. Let us now consider the case  $L_y = 2$ . The Möbius strip corresponds to the  $U = \sigma_x$  case, which has determinant  $-1$ . Therefore, can not be connected continuously to the identity matrix. On the other hand, one can reach a pseudo-Möbius strip using a rotation of  $\pi$ ,  $U_{1,2} = -U_{2,1} = 1$ .

### III. COLD ATOM IMPLEMENTATION

In this section, we show how the artificial topologies described previously can be made concrete, for instance, in a cold atom set-up. The basic features that allow to realize the abstract construction of sect. II in a cold atom system are the following:

- the synthetic lattice is obtained by loading in a 1D (spin-independent) optical lattice the atoms, whose hyperfine states, belonging to a unique or few hyperfine manifolds, provide internal species which form the synthetic dimension;
- the hopping term  $J_{i,\sigma,\sigma'}^h$  of (2) is the free hopping of atoms in the 1D optical lattice and is naturally spin-independent,  $J_{i,\sigma,\sigma'}^h = J \delta_{\sigma,\sigma'}$ , as assumed in the construction of Hamiltonians (3) and (7) and their periodic completions;
- the hopping term  $J_{i,\sigma,\sigma'}^v$  is induced and tailored by laser and radiofrequency couplings which are local

in the real-space picture, i.e., are acting on a single site of the 1D chain.

A similar dictionary can be obtained for other platforms. For instance, in the spirit of [53], a synthetic dimension can be achieved also in photonic crystals as in [74, 75], by changing the connectivity of the lattice.

It is worth to notice that, while the real spatial dimension is virtually “unlimited” (or better scaled up to order  $10^2$  lattices sites), the synthetic dimension is limited always by the number of atomic internal states available, which is up to 10 for standard atoms like  $^{40}\text{K}$  or  $^{87}\text{Sr}$  [76], but can be up to 20 in  $^{167}\text{Er}$  [77], if just one hyperfine manifold is taken into account. However, by considering more than one hyperfine manifold simultaneously or ultracold molecules, see e.g., [78], this number can be further increased. A limited synthetic dimension translates into a limited transverse dimension of the artificial topology.

Let us start by discussing how to implement the building block of our construction, a (spinless) periodic chain from a (spinful) open one. In cold atoms, model (2) applied to create PBC can be realized for instance by loading atoms with at least two hyperfine (almost degenerate) ground states ( $F \geq \frac{1}{2}$ ) in a spin-independent quasi-1D optical lattice of  $L$  sites. The free tunneling provides the terms in  $J^h$ , while the terms in  $J^v$  can be created using Rabi oscillations between the hyperfine states, induced by Raman lasers focused on sites 1 and  $L$ , respectively. Thus, the synthetic approach we are proposing is essentially local, since the different species are physically at the same site. Notice the *scalability* of the procedure: we can build PBC 1D systems of any size  $2L$ , if we can build an associated open system with  $L$  sites and  $M = 2$  internal states.

#### A. Cylinder and Torus

Let us extend the above construction to the simulation of a cylinder by layering many circles together as explained in sect. II A. It is easy to realize that the Hamiltonian of (3) can be implemented with up to two-photon transitions. Indeed, the most direct arrangement of the internal degrees of freedom  $\sigma$  is in terms of hyperfine states within a unique hyperfine manifold  $F \geq \frac{L_y-1}{2}$ , e.g.,  $|\sigma\rangle = b^{(\sigma)\dagger}|0\rangle = |F, m_F = \bar{m} + \sigma\rangle$ . For this ordering of the spins, the synthetic sewing coupling  $C_{\sigma\sigma'}$  applied at real-space sites  $i = 1$  and  $i = L$  requires  $\Delta m_F = 1$ , while the synthetic transverse coupling  $B_{\sigma\sigma'}$  requires  $\Delta m_F = 2$  for any  $L_y$ . Thus, the only limitation in  $L_y$  is given by the number of available internal states. It is worth to notice that the coupling  $C_{\sigma\sigma'}$  applies only alternatively, i.e., it connects only odd and even spin values. This implies that the hyperfine states have to be spectroscopically distinguishable, for instance, through a quadratic Zeeman splitting.

The spin arrangement considered above is not the only

possible one. Furthermore, two or more (meta)stable hypermanifolds can be considered. Such a construction is particularly favorable in earth-alkali like atoms like Yb (see e.g., [79–82]) where the optically connected  $^1S_0$  and the  $^3P_0$  may be used. In this case, a convenient arrangement is to place odd (even)  $\sigma$ 's in the first (second) manifold, i.e.,  $|2\sigma\rangle = b^{(2\sigma)\dagger}|0\rangle = |I, F, m_F = \bar{m} + \sigma\rangle$ ,  $(|2\sigma + 1\rangle = b^{(2\sigma+1)\dagger}|0\rangle = |II, F, m_F = \bar{m} + \sigma\rangle)$ . Thus, the Hamiltonian (3) involves in this scheme just  $\Delta m_F = 1$  transitions. As further discussed below (cf. sect. III C), the two-manifold construction allows for a richer interaction pattern than single-manifold one. Both schemes are depicted in Fig. 3.

Let us now turn to the implementation of a torus geometry. As described in sect. II A, further couplings are needed, which connect the top and the bottom circles. In the synthetic-lattice basis, this is equivalent to connecting the last of the odd (even) spins with the first odd (even) one, for any real-space site. Such a construction makes sense when  $L_y$  is at least 3, the case whose implementation is detailed in Fig. 4. For simplicity, let us focus on the two-manifold construction. Here, the additional coupling requires just  $\Delta m_F = 2$  and, similarly to the periodic boundary conditions engineered in [30], can be achieved for instance via a 3-photon transition. For generic  $L_y$ , the needed transition has  $\Delta m_f = L_y - 1$ .

### B. Möbius and Twisted Torus

Let us now discuss the cold atom implementation of a Möbius strip. As explained in sect. II B, we can get a Möbius from the cylinder by replacing the synthetic coupling  $C_{\sigma\sigma'}$ , at (e.g.) real-space site  $i = 1$  with the coupling  $C_{\sigma\sigma'}^M$ . This is equivalent to connecting the internal states  $|\sigma = 2l\rangle$  with  $|2(L_y + 1 - l)\rangle$ , and the states  $|\sigma = 2l - 1\rangle$  with  $|2(L_y - l) + 1\rangle$ , for  $l = 1, \dots, L_y$ . It is immediate to realize that for any arrangement of the internal states as hyperfine states (both in the one- and two-manifold scenarios) this implies that the maximum  $\Delta m_f$  needed to engineer  $C_{\sigma\sigma'}^M$  scales with  $L_y$ . For instance, in the two-manifold scheme with the arrangement for the  $\sigma$ 's described above, the maximal  $\Delta m_F$  is exactly  $L_y$ , see Fig. 5 c). Thus, the feasible transverse dimension of the strip is technically limited, let us say to  $L_y = 4$ , value which requires at least four-photon transitions.

The step to the implementation of a twisted torus is quite easy and requires the addition of a coupling with  $\Delta m_F = L_y - 1$ , as described above.

### C. Interactions

The constructions we have presented produced the kinetic terms of the Hamiltonians, which are indeed the relevant part for the connectivity of the model (including boundary conditions) and, thus, for the hoppings. Cold atom implementation provides a natural way of in-

cluding interactions. In the synthetic-lattice picture, ordinary on-site interactions due to collisions of atoms with different spins appear as long-ranged.

The pattern of such long-range interactions can be partially controlled. For instance, it is potentially very different for in the (i) one-manifold and in the (ii) two-manifold schemes. Interactions between hyperfine states of the same manifold may change a lot from atom to atom, but the non-spin-changing ones are in general all of the same order of magnitude and, for earth-alkali atoms, they are equal. The spin-changing ones are naturally suppressed ( $p$ -wave) and can be enhanced without inducing too high three-body losses by using optical Feshbach resonances [83–85]. An alternative route is given by Raman-induced interactions near  $s$ -wave Feshbach resonance [86–88]. Collisions between atoms in different manifolds are not affected by such constraint but are in general lossy.

Let us start discussing in details the case (i) with the assumption of  $SU(2F + 1)$ -symmetric interactions  $H_I = \frac{U}{2} \sum_j \hat{n}_j(\hat{n}_j - 1)$ , where  $\hat{n}_j = \sum_{\sigma=1,2L} b_j^{(\sigma)\dagger} b_j^{(\sigma)}$  is the total occupation on site  $j$  of the physical 1D-chain. As the interaction is invariant under reordering of the spins, the final Hubbard model on the synthetic cylinder and the Möbius strip looks the same for any of the arrangements chosen to represent the  $\sigma$  in terms of  $m_F$ . Indeed, supposing that we selectively fill only the spin-states needed i.e.,  $2L_y$ , the local occupation at site  $j$  of the chain becomes the sum of local occupations at sites  $r = j$  and  $r' = 2L_x + 1 - j$  of the synthetic lattice,  $\hat{n}_j = \sum_{l=1}^{L_y} (a_{r,l}^\dagger a_{r,l} + a_{r',l}^\dagger a_{r',l})$ . Thus, the interactions will be full range in the transverse direction at fixed  $r$  and for pairs  $(r, 2L_y + 1 - r)$ ,  $H_I = \frac{U}{2} \sum_{r=1}^{2L_x} (\hat{N}_r(\hat{N}_r - 1) + \hat{N}_r \hat{N}_{2L_x+1-r})$ , where  $\hat{N}_r \equiv \sum_{l=1}^{L_y} a_{r,l}^\dagger a_{r,l}$ .

The situation is quite different in scenario (ii), even under the assumption that the interactions are  $SU(2F + 1)$ -invariant in each hyperfine manifold. To be definite let us consider earth-alkali like atoms and assume that interactions are negligible in each hyperfine manifold with respect to the inter-manifold ones, which we model to be just density-density. The final  $H_I$ -term in the synthetic lattice is strongly dependent on the chosen spin arrangement. For instance, we can engineer a model where only the term  $\frac{U}{2} \sum_r \hat{N}_r \hat{N}_{2L_x+1-r}$  appears.

## IV. TOPOLOGY SIGNATURES

Let us discuss possible experimental signatures of the topology of the underlying manifold showing up in quantum many-body dynamics which are amenable to experimental observation in our synthetic lattices.

We start by discussing the simplest paradigmatic example of a line with two species which can be designed to mimic a single species Hamiltonian on a circumference, as described in Sect. II. In order to illustrate this idea in a simple way, let us consider the following Hamilto-

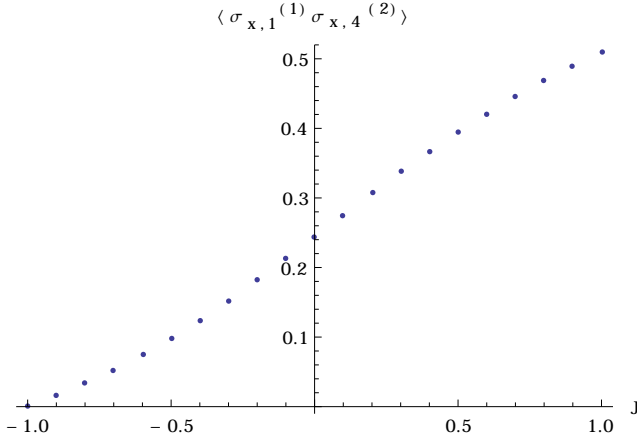


FIG. 7. Two four-spin Ising chains can be turned into a single chain of eight spins by tuning the boundary couplings, as shown in Eq. 11. The plot shows the correlation of spins of each species at the different boundaries,  $B$ , as a function of the coupling  $J_L \in [-1, 1]$ , for  $J_1 = \lambda = 1$ . Note the cancellation of correlations in the case of an artificially frustrated boundary.

nian for a double spin chain of length  $L$ , with tunable connecting terms at the boundaries:

$$\begin{aligned}
 H = & \sum_{i=1}^{L-1} \sigma_{i,1}^x \sigma_{i+1,1}^x + \lambda \sum_{i=1}^L \sigma_{i,1}^z \\
 & + \sum_{i=1}^{L-1} \sigma_{i,2}^x \sigma_{i+1,2}^x + \lambda \sum_{i=1}^L \sigma_{i,2}^z \\
 & + J_1 \sigma_{1,1}^x \sigma_{1,2}^x + J_L \sigma_{L,1}^x \sigma_{L,2}^x.
 \end{aligned} \quad (10)$$

where  $\sigma_{i,m}^k$  denotes the  $k$ -th component of the spin on site  $i$ , rung  $m$ . The two closing interactions  $J_1$  and  $J_L$  are responsible for turning the two open chains into a single one on a circumference. As a consequence, boundary conditions are dictated by these coefficients. A signature of the artificial boundary conditions can be measured by the correlation between spins on different chains at a boundary, namely:

$$B \equiv \langle \sigma_{1,1}^x \sigma_{L,2}^x \rangle - \langle \sigma_{1,1}^x \rangle \langle \sigma_{L,2}^x \rangle. \quad (11)$$

Observable  $B$  should be zero for disconnected chains. Its value for fixed  $J_1 = 1$  and  $J \equiv J_L \in [-1, 1]$  is shown in Fig. 7 for  $L = 4$  and  $\lambda = 1$ . Notice that  $J = 1$  corresponds to the PBC case, which maximally entangles both chains and gives the highest correlator. For  $J = 0$ , we obtain a single open BC chain. More interestingly, for  $J = -1$ , the twist in the boundary condition induces a perfect cancellation in the correlator. This effect is, indeed, a signature of the non-triviality of the topological effects.

Nonetheless, realistic simulations should model the underlying geometry by tuning the hoppings of fermions or bosons. We shall now address such cases, looking for both single-particle and interacting signatures.

## A. Single-Particle signatures

A natural single-particle playground where we can observe the effect of the topology is to consider synthetic magnetic fluxes, which boils down to hoppings with non-trivial phases. In our synthetic lattice it is very easy to control such phases, in particular to make them linearly dependent with the position on the chain if the synthetic links are induced through Raman lasers.

Let us start with a 1D Hamiltonian with PBC, as in Eq. (1), either for spinless fermions or bosons, with an arbitrary closing phase  $J_c = e^{i\phi}$ , representing a magnetic flux. Its single-particle spectrum, as a function of  $\phi \in [0, 2\pi]$  is shown in Fig. 8. Thus, the left and right extremes are periodic boundary conditions, while the center corresponds to anti-periodic ones. Notice that the gap of a fermionic system at half-filling will evolve continuously, presenting a maximum at  $\phi = \pi$ .

The more involved case of a 2-rung ladder is shown in Fig. 8 (b) and (c). In those cases we have again a free Hamiltonian either for spinless fermions or bosons, such as Eq. (3) with  $L_y = 2$ . The closing link between the two extremes can be chosen to be a generic unitary matrix, as shown in Eq. (9). In both cases, we have selected a one-parameter family of unitary matrices with special properties. In 8 (b) it is a rotation of angle  $\phi$ :

$$U_{+1}(\phi) = \begin{pmatrix} \cos \phi & -\sin \phi \\ \sin \phi & \cos \phi \end{pmatrix} \quad (12)$$

where the  $+1$  stands for the value of the determinant. Thus, for  $\phi = 0$  we have the identity matrix, which means cylindrical boundary conditions. Meanwhile, for (c) we have used a different one-parameter family:

$$U_{-1}(\phi) = \begin{pmatrix} \cos \phi & \sin \phi \\ \sin \phi & -\cos \phi \end{pmatrix} \quad (13)$$

Although those transformations are unitary, they have determinant  $-1$ , and thus can not be connected continuously with the identity matrix. For  $\phi = \pi$  we obtain a Möbius strip. Notice that the single-particle spectrum is different in both cases, and thus the energy gap at half-filling constitute a topological signature.

The magnetic single-particle behavior is sensitive to the orientability of the underlying lattice. If the lattice is topologically equivalent to a cylinder and orientable, a constant magnetic field piercing the surface induces steady counter-propagating currents on each edge, which are called edge states. Their topological nature reflects on their robustness under local perturbations. If the lattice is not orientable, intuition dictates that the current cannot form as there is no notion of normal to the lattice, i.e., of sign of the magnetic flux and thus of chirality of the currents. We can check our intuition by considering the synthetic cylinder and Möbius strip as examples of orientable and no-orientable surface with sharp boundaries, respectively. Our synthetic construction allows to

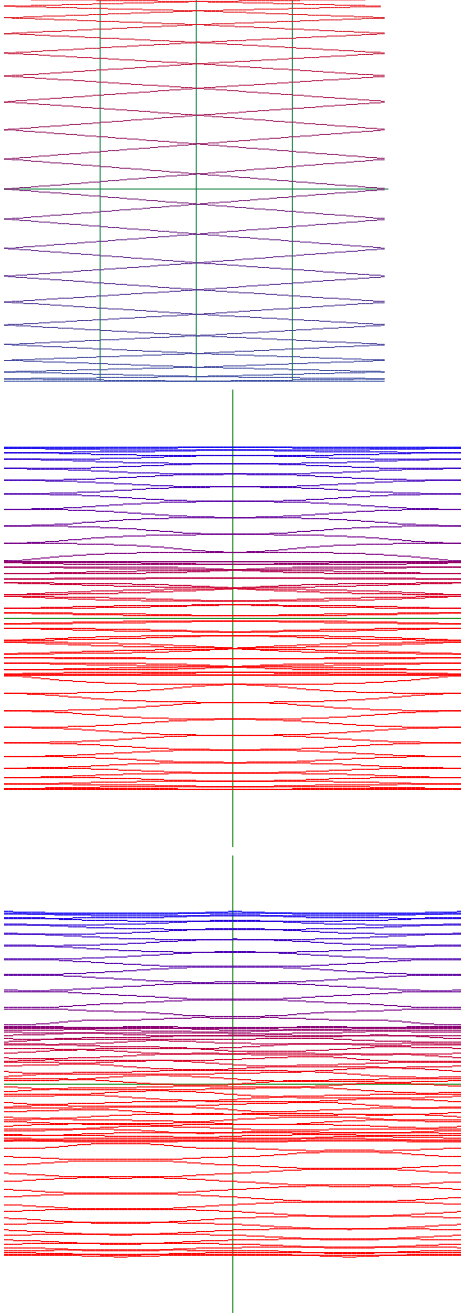


FIG. 8. Hofstadter-like single-particle spectra of several quasi-1D systems under a continuous change of boundary conditions. In all cases the  $X$ -axis is labeled by  $\phi \in [0, 2\pi]$ , and color corresponds to eigenvalue index. In (a) we present the spectrum for a PBC system such as that in Eq. (1) with  $L = 40$ , pierced with a flux  $J_c = e^{i\phi}$  with  $\phi \in [0, 2\pi]$ . In (b) and (c) we show the single-body spectrum of a ladder of size  $40 \times 2$ , such as Eq. (3) in which the opposite extremes are joined with a unitary matrix of different types: cylindrical in (b) and Möbius-like in (c), as specified in the boundary conditions given in equations (12) and (13).

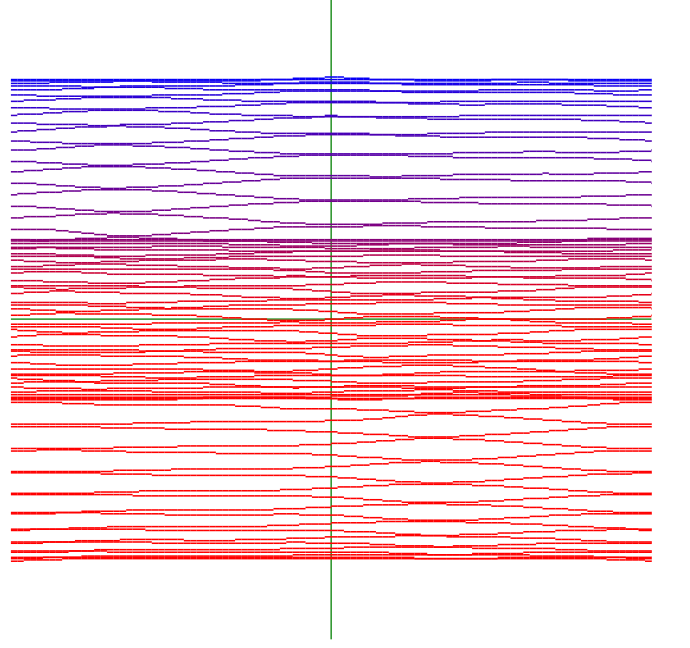


FIG. 9. Single-particle spectrum of the  $40 \times 2$  ladder Hamiltonian represented in Eq. (3) undergoing a smooth transition between a cylinder and a Möbius strip, with boundary conditions specified in Eq. (14).

smoothly interpolate between the two by considering a  $U$  matrix of the form

$$U_{+1 \rightarrow -1}(\phi) = \begin{pmatrix} \cos \phi & -\sin \phi e^{i\phi} \\ \sin \phi & \cos \phi e^{i\phi} \end{pmatrix} \quad (14)$$

this hopping matrix is also unitary, but its determinant is  $e^{i\phi}$ . For  $\phi = 0$  it is  $+1$ , and we have the cylinder, while for  $\phi = \pi$  it gets  $-1$ , and we obtain the Möbius strip. The single-particle spectrum of this  $L_x \times 2$  ladder with different boundary conditions is shown in Fig. 9.

## B. Interacting signatures

Quantum simulators are not restricted to the study of free systems. Interactions can typically be tailored to a certain extent. Our generic Hamiltonian can be written as

$$H = H_K + U \sum_{\langle i,j \rangle} n_i n_j - \sum_i \mu_i n_i, \quad (15)$$

where  $H_K$  is the kinetic Hamiltonian described in Eq. (2), and  $U$  is the strength of the nearest-neighbor interaction,  $\mu_i$  is a local chemical potential and  $n_i$  is the local particle number. The sum in the second term is over nearest neighbors of a certain adjacency structure, which need not be the same as the one employed for the

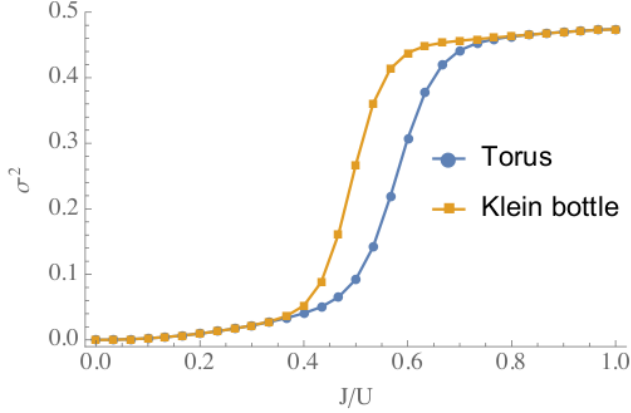


FIG. 10. Ground state particle-number fluctuations for the Bose-Hubbard model of Eq. 15 at half filling, defined on a 2D lattice with periodic boundary conditions in both directions – a torus – and on a 2D lattice with the boundary conditions of a Klein bottle, computed via exact diagonalization. The results are for a 4x4 lattice. Similarly to the results for the Möbius band, the ground state in twisted boundary conditions seems to favor larger particle-number fluctuations at intermediate values of  $J/U$ . The computation has been done with small disorder in  $\mu$  to remove the degeneracy at  $J = 0$ , as the two complementary checkerboard coverings of the lattice are ground states.

kinetic term. We take  $\mu_i$  to be slightly random, in order to remove exact degeneracy in the ground state. The topology of the underlying lattice are totally encoded in the kinetic Hamiltonian  $H_K$ , which is affected by a global hopping constant  $J$ .

Let us start by considering a bosonic system with Hamiltonian (15) and focus on the local particle-number fluctuations in the ground state,  $\sigma^2 = \sum_i (\langle n_i^2 \rangle - \langle n_i \rangle^2) / N$ , where  $N$  is the total particle number. It can be employed to distinguish the different phases. Mean-field calculations cannot distinguish between different topologies, since they are local in character so, *a fortiori*, it will give the same estimate for  $\sigma^2$  for all boundary conditions. Using exact diagonalization, on the other hand, different topologies can be told apart by inspecting the behavior of  $\sigma^2$  as a function of  $J/U$ . For a large  $J/U$  the bosons are in a superfluid state with large particle-number fluctuations, since each particle is delocalized over the whole lattice. For small  $J/U$  the bosons are localized in a checkerboard pattern and the particle-number fluctuations are small.

We consider different boundary conditions for compact lattices (torus and Klein bottle) and open lattices (cylinder and Möbius strip) for different sizes. In Fig. 11 we

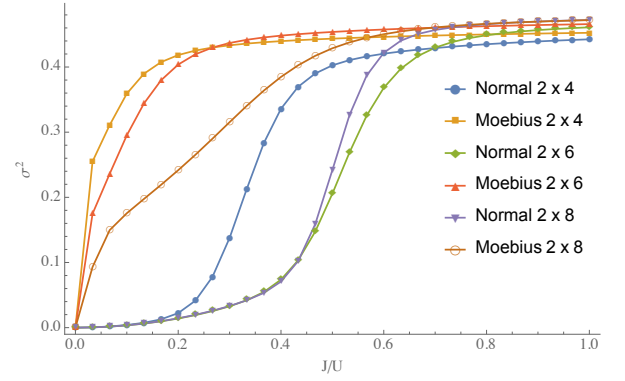


FIG. 11. Particle-number fluctuations in the ground state of the Bose-Hubbard model of Eq. (15) at half filling defined on a strip with periodic and Möbius boundary conditions computed with exact diagonalization. The results are for strips 4, 6 and 8 sites long. For large interactions compared to the hopping parameter the ground state presents larger particle-number fluctuations for twisted boundary conditions than for regular ones. This behavior does not disappear as the system size increases, for the range of sizes analyzed. The computation has been done with small disorder in  $\mu$  to remove spurious degeneracy.

plot  $\sigma^2$  as a function of  $J/U$  for the normal strip and the Möbius strip for different strip lengths. As expected, in the limits  $J/U \rightarrow 0$  and  $J/U \rightarrow 1$  the ground state has the same boson number fluctuations, which is explained by the fact that in both limits the ground state is a product state in the site basis [89]. In the latter limit this is not exactly the case due to finite size effects. The data shows that for intermediate values of  $J/U$ , where the ground state is entangled,  $\sigma^2$  is sensitive to the different boundary conditions. In Fig. 10 we plot  $\sigma^2$  for the ground state of the Bose-Hubbard model on a torus and on a Klein bottle. The data shows that  $\sigma^2$  can tell the different boundary conditions apart in this case as well for intermediate values of  $J/U$ .

Let us now consider a fermionic system with two species per site and a slightly different dynamics. Let (15) still be the Hamiltonian, but we make the repulsion term work only along vertical lines, i.e., only between particles in the same real-space site. In terms of the synthetic lattice we can write

$$H = H_K + U \sum_{i=1}^{L_x} n_i^{(1)} n_i^{(2)} + H.c. \quad (16)$$

For an even  $L_x$  we have studied the ground state and first excited state of Hamiltonian (16) on a cylinder and Möbius strip. The first is characterized by the independent motion of each species. The second by a crossing at the end, where the species transmute.

Some results are shown in Fig. 12, for  $U=J$ . From top to bottom we see panels (a) and (b), which depict the

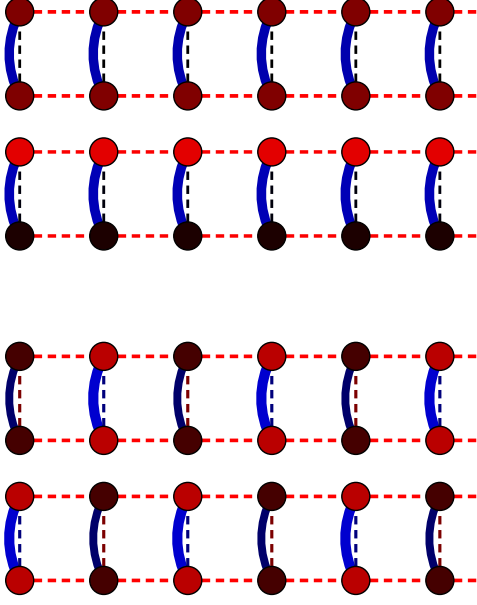


FIG. 12. Representation of the ground state and first excited state of the fermionic Hubbard model (16) on a cylinder and a Möbius strip of size  $L_x = 6$  and  $L_y = 2$ . The repulsion only takes place along the same rung. The color of each node represents the expected value of  $\langle n_i \rangle$ . The color of the bent line represents the correlator  $\langle n_i n_j \rangle - \langle n_i \rangle \langle n_j \rangle$ . The dashed lines are the correlators  $\langle a_i^\dagger a_j \rangle$ .

ground state and first excited state for the cylinder, and panels (c) and (d) which show the corresponding Möbius states. The color of the circles represent the density,  $\langle n_i \rangle$ , while the colored arcs represent the density-density correlator:  $\langle n_i n_j \rangle - \langle n_i \rangle \langle n_j \rangle$ . The dashed lines represent the hopping correlator,  $\langle a_i^\dagger a_j \rangle$ , red being positive and blue negative in all cases.

The ground state of the cylinder, panel (a) of 12 is characterized by a homogeneous density and density-density correlators. The first excited state, shown in figure (b) is doubly degenerate, and it is obtained by adding one more particle at the upper species. Particles never move between species, as shown in the null vertical hopping correlators. The physical picture can be described as follows. The particles move along their lines in counter-phase, i.e., with highly negative density-density correlator between the two *lines*. This does not lead to frustration because  $L_x$  is even and the lanes never cross.

Panels (c) and (d) show the situation for the Möbius topology. The ground state is degenerate, and both states are depicted there. The local density now shows a checkered pattern, and also the density-density correlators. The vertical hopping correlators show also an interesting pattern, alternating positive and negative values. The physical picture is as follows. The lane crossing

induced by topology makes impossible the previous configuration due to frustration. The two lanes have become one, and the only possibility to reduce vertical repulsion is to freeze the system into a charge-density wave. Particles can not move as fast as they would like to reduce their kinetic energy, which is an analogue of a *traffic jam*. That is the reason for the lane changing correlators.

Combining the information of Fig. 12 we see that the Mott transition takes place at different values of the  $J/U$  parameter, independently of the system size. This effect is related in a non-trivial way to frustration.

## V. CONCLUSIONS

We have shown that non-trivial topologies can be simulated by a combination of two techniques, namely the use of several species at every spatial degrees of freedom and the generation of couplings among these species only at the boundaries of the system. In other words, species work as an extra dimension that allows for the generation of topological transformations from localized interactions.

In particular we have presented explicit proposals for the realization of the following geometries:

- a circle
- a cylinder
- a torus
- a Möbius strip
- a twisted torus

We have discussed different possibilities of experimental realization of the proposed schemes, extending significantly the ideas of Ref. [53]. Finally, we have presented several signatures of the underlying lattice topology both on free and interacting systems. These examples involve synthetic gauge fields and synthetic dimension, including:

- A two-species open Ising chain with localized interactions among them can be converted in a double-length single-species chain with a synthetic magnetic field.
- Hofstadter-like spectra can be obtained for a circle, a cylinder and a Möbius strip.
- Hubbard systems of moderate size can be engineered on a torus, a Klein bottle, a cylinder and a Möbius strip.

Our findings open paths to further investigations of both free and weakly interacting, as well as strongly correlated systems in optical lattices with non-trivial topology. Combining such lattice geometries with synthetic gauge fields leads to various spectacular effects that are within the reach of current experiments.

## ACKNOWLEDGMENTS

We acknowledge useful discussions with S. Iblisdir, P. Massignan and L. Tagliacozzo, and financial support from FIS2013-41757-P, FIS2012-33642, ERC AdG OSYRIS, EU IP SIQS, EU STREP EQuaM, and Fundació CELLEX. O.B. acknowledges support

from Fundação para a Ciência e a Tecnologia (Portugal), namely through programmes PTDC/POP and projects PEst-OE/EGE/UI0491/2013, PEst-OE/EEI/LA0008/2013, IT/QuSim and CRUP-CPU/CQVibes, partially funded by EU FEDER, and from the EU FP7 projects LANDAUER (GA 318287) and PAPETS (GA 323901).

- 
- [1] M. Lewenstein, A. Sanpera, and V. Ahufinger, *Ultracold Atoms in Optical Lattices: Simulating quantum many-body systems* (Oxford University Press, 2012).
  - [2] J. Dalibard, F. Gerbier, G. Juzeliūnas, and P. Öhberg, *Rev. Mod. Phys.* **83**, 1523 (2011).
  - [3] E. Zohar, J. I. Cirac, and B. Reznik, *Phys. Rev. Lett.* **109**, 125302 (2012).
  - [4] D. Banerjee, M. Dalmonte, M. Müller, E. Rico, P. Stebler, U.-J. Wiese, and P. Zoller, *Phys. Rev. Lett.* **109**, 175302 (2012).
  - [5] L. Tagliacozzo, A. Celi, A. Zamora, and M. Lewenstein, *Ann. Phys.* **330**, 160 (2013).
  - [6] E. Zohar, J. I. Cirac, and B. Reznik, *Phys. Rev. Lett.* **110**, 125304 (2013).
  - [7] D. Banerjee, M. Bögli, M. Dalmonte, E. Rico, P. Stebler, U.-J. Wiese, and P. Zoller, *Phys. Rev. Lett.* **110**, 125303 (2013).
  - [8] L. Tagliacozzo, A. Celi, P. Orland, M. W. Mitchell, and M. Lewenstein, *Nature Comm.* **4** (2013).
  - [9] I. Bloch, J. Dalibard, and S. Nascimbène, *Nature Phys.* **8**, 267 (2012).
  - [10] R. Blatt and C. Roos, *Nature Phys.* **8**, 277 (2012).
  - [11] A. Aspuru-Guzik and P. Walther, *Nature Phys.* **8**, 285 (2012).
  - [12] J. Cai, A. Retzker, F. Jelezko, and M. B. Plenio, *Nature Phys.* **9**, 168 (2013).
  - [13] A. A. Houck, H. E. Türeci, and J. Koch, *Nature Phys.* **8**, 292 (2012).
  - [14] F. Haldane and M. Duncan, *Phys. Rev. Lett.* **61**, 2015 (1988).
  - [15] J. J. Sakurai and J. Napolitano, *Modern quantum mechanics* (Addison-Wesley, 2011).
  - [16] W. Su, J. R. Schrieffer, and A. J. Heeger, *Phys. Rev. Lett.* **42**, 1698 (1979).
  - [17] R. Jackiw and C. Rebbi, *Phys. Rev. D* **13**, 3398 (1976).
  - [18] E. Witten, *Nuclear Physics B* **156**, 269 (1979).
  - [19] G. Veneziano, *Nuclear Physics B* **159**, 213 (1979).
  - [20] M. Z. Hasan and C. L. Kane, *Rev. Mod. Phys.* **82**, 3045 (2010).
  - [21] C. Nayak, S. H. Simon, A. Stern, M. Freedman, and S. D. Sarma, *Rev. Mod. Phys.* **80**, 1083 (2008).
  - [22] A. Y. Kitaev, *Ann. Phys.* **303**, 2 (2003).
  - [23] H. Weimer, M. Müller, I. Lesanovsky, P. Zoller, and H. P. Büchler, *Nature Phys.* **6**, 382 (2010).
  - [24] J. T. Barreiro, M. Müller, P. Schindler, D. Nigg, T. Monz, M. Chwalla, M. Hennrich, C. F. Roos, P. Zoller, and R. Blatt, *Nature* **470**, 486 (2011).
  - [25] T. Kitagawa, E. Berg, M. Rudner, and E. Demler, *Phys. Rev. B* **82**, 235114 (2010).
  - [26] T. Kitagawa, M. A. Broome, A. Fedrizzi, M. S. Rudner, E. Berg, I. Kassal, A. Aspuru-Guzik, E. Demler, and A. G. White, *Nature Comm.* **3**, 882 (2012).
  - [27] J. K. Asbóth and H. Obuse, *Phys. Rev. B* **88**, 121406 (2013).
  - [28] N. Goldman, J. Beugnon, and F. Gerbier, *Phys. Rev. Lett.* **108**, 255303 (2012).
  - [29] D. Hügel and B. Paredes, *Phys. Rev. A* **89**, 023619 (2014).
  - [30] A. Celi, P. Massignan, J. Ruseckas, N. Goldman, I. B. Spielman, G. Juzeliūnas, and M. Lewenstein, *Phys. Rev. Lett.* **112**, 043001 (2014).
  - [31] M. Atala, M. Aidelsburger, M. Lohse, J. T. Barreiro, B. Paredes, and I. Bloch, *Nature Physics* **10**, 588 (2014).
  - [32] N. Goldman, I. Satija, P. Nikolic, A. Bermudez, M. Martin-Delgado, M. Lewenstein, and I. Spielman, *Phys. Rev. Lett.* **105**, 255302 (2010).
  - [33] P. Hauke, O. Tieleman, A. Celi, C. Ölschläger, J. Simonet, J. Struck, M. Weinberg, P. Windpassinger, K. Sengstock, M. Lewenstein, *et al.*, *Phys. Rev. Lett.* **109**, 145301 (2012).
  - [34] M. Beeler, R. Williams, K. Jimenez-Garcia, L. LeBlanc, A. Perry, and I. Spielman, *Nature* **498**, 201 (2013).
  - [35] G. Jotzu, M. Messer, R. Desbuquois, M. Lebrat, T. Uehlinger, D. Greif, and T. Esslinger, *arXiv preprint arXiv:1406.7874* (2014).
  - [36] J. Struck, J. Simonet, and K. Sengstock, *arXiv preprint arXiv:1407.1953* (2014).
  - [37] L. Fu and C. L. Kane, *Phys. Rev. Lett.* **100**, 096407 (2008).
  - [38] V. Mourik, K. Zuo, S. Frolov, S. Plissard, E. Bakkers, and L. Kouwenhoven, *Science* **336**, 1003 (2012).
  - [39] L. Jiang, T. Kitagawa, J. Alicea, A. Akhmerov, D. Pekker, G. Refael, J. I. Cirac, E. Demler, M. D. Lukin, and P. Zoller, *Phys. Rev. Lett.* **106**, 220402 (2011).
  - [40] R. Kanamoto, L. D. Carr, and M. Ueda, *Phys. Rev. A* **79**, 063616 (2009).
  - [41] L. D. Carr, C. W. Clark, and W. P. Reinhardt, *Phys. Rev. A* **62**, 063610 (2000).
  - [42] L. D. Carr, C. W. Clark, and W. P. Reinhardt, *Phys. Rev. A* **62**, 063611 (2000).
  - [43] A. Ramanathan, K. C. Wright, S. R. Muniz, M. Zelan, W. T. Hill III, C. J. Lobb, K. Helmerson, W. D. Phillips, and G. K. Campbell, *Phys. Rev. Lett.* **106**, 130401 (2011).
  - [44] S. Eckel, F. Jendrzejewski, A. Kumar, C. Lobb, and G. Campbell, *arXiv preprint arXiv:1406.1095* (2014).
  - [45] F. Jendrzejewski, S. Eckel, N. Murray, C. Lanier, M. Edwards, C. J. Lobb, and G. K. Campbell, *Phys. Rev. Lett.* **113**, 045305 (2014).
  - [46] K. C. Wright, R. B. Blakestad, C. J. Lobb, W. D. Phillips, and G. K. Campbell, *Phys. Rev. A* **88**, 063633 (2013).
  - [47] N. Murray, M. Krygier, M. Edwards, K. C. Wright, G. K. Campbell, and C. W. Clark, *Phys. Rev. A* **88**, 053615 (2013).

- (2013).
- [48] K. C. Wright, R. B. Blakestad, C. J. Lobb, W. D. Phillips, and G. K. Campbell, Phys. Rev. Lett. **110**, 025302 (2013).
  - [49] A. Ramanathan, K. C. Wright, S. R. Muniz, M. Zeilan, W. T. Hill, C. J. Lobb, K. Helmerson, W. D. Phillips, and G. K. Campbell, Phys. Rev. Lett. **106**, 130401 (2011).
  - [50] W. Beugeling, A. Quelle, and C. M. Smith, Phys. Rev. B **89**, 235112 (2014).
  - [51] A. Quelle, W. Beugeling, and C. M. Smith, arXiv:1408.3087.
  - [52] O. Boada, A. Celi, J. I. Latorre, and M. Lewenstein, New J. Phys. **13**, 035002 (2011).
  - [53] O. Boada, A. Celi, J. I. Latorre, and M. Lewenstein, Phys. Rev. Lett. **108**, 133001 (2012).
  - [54] C. Ryu, M. F. Andersen, P. Cladé, V. Natarajan, K. Helmerson, and W. D. Phillips, Phys. Rev. Lett. **99**, 260401 (2007).
  - [55] J. Brand and W. P. Reinhardt, Journal of Physics B: Atomic, Molecular and Optical Physics **34**, L113 (2001).
  - [56] M. Abad, A. Sartori, S. Finazzi, and A. Recati, Phys. Rev. A **89**, 053602 (2014).
  - [57] S. Baharian and G. Baym, Phys. Rev. A **87**, 013619 (2013).
  - [58] L. A. Toikka and K.-A. Suominen, Phys. Rev. A **87**, 043601 (2013).
  - [59] M. Abad, M. Guilleumas, R. Mayol, M. Pi, and D. M. Jezek, Phys. Rev. A **81**, 043619 (2010).
  - [60] P. Mason and N. G. Berloff, Phys. Rev. A **79**, 043620 (2009).
  - [61] M. Ogren and G. Kavoulakis, Journal of Low Temperature Physics **154**, 30 (2009).
  - [62] A. D. Jackson and G. M. Kavoulakis, Phys. Rev. A **74**, 065601 (2006).
  - [63] T. Fernholz, R. Gerritsma, P. Krüger, and R. J. C. Spreeuw, Phys. Rev. A **75**, 063406 (2007).
  - [64] A. Parola, L. Salasnich, R. Rota, and L. Reatto, Phys. Rev. A **72**, 063612 (2005).
  - [65] A. B. Bhattacharjee, E. Courtade, and E. Arimondo, Journal of Physics B: Atomic, Molecular and Optical Physics **37**, 4397 (2004).
  - [66] T. Schulte, L. Santos, A. Sanpera, and M. Lewenstein, Phys. Rev. A **66**, 033602 (2002).
  - [67] E. M. Wright, J. Arlt, and K. Dholakia, Phys. Rev. A **63**, 013608 (2000).
  - [68] L. Salasnich, A. Parola, and L. Reatto, Phys. Rev. A **59**, 2990 (1999).
  - [69] M. Benakli, S. Raghavan, A. Smerzi, S. Fantoni, and S. R. Shenoy, EPL (Europhysics Letters) **46**, 275 (1999).
  - [70] W. S. Bakr, J. I. Gillen, A. Peng, S. Fölling, and M. Greiner, Nature **462**, 74 (2009).
  - [71] J. F. Sherson, C. Weitenberg, M. Endres, M. Cheneau, I. Bloch, and S. Kuhr, Nature **467**, 68 (2010).
  - [72] F. C. Alcaraz, M. N. Barber, and M. T. Batchelor, Phys. Rev. Lett. **58**, 771 (1987).
  - [73] F. C. Alcaraz, M. N. Barber, and M. T. Batchelor, Ann. Phys. **182**, 280 (1988).
  - [74] D. Jukić and H. Buljan, Phys. Rev. A **87**, 013814 (2013).
  - [75] J. M. Edge, J. Tworzydło, and C. W. J. Beenakker, Phys. Rev. Lett. **109**, 135701 (2012).
  - [76] S. Stellmer, R. Grimm, and F. Schreck, Phys. Rev. A **87**, 013611 (2013).
  - [77] K. Aikawa, A. Frisch, M. Mark, S. Baier, R. Grimm, and F. Ferlaino, Phys. Rev. Lett. **112**, 010404 (2014).
  - [78] M. Wall, K. Maeda, and L. Carr, arXiv:1402.0465.
  - [79] G. Pagano, M. Mancini, G. Cappellini, P. Lombardi, F. Schäfer, H. Hu, X.-J. Liu, J. Catani, C. Sias, M. Inguscio, *et al.*, Nature Phys. (2014).
  - [80] G. Cappellini, M. Mancini, G. Pagano, P. Lombardi, L. Liv, M. S. de Cumis, P. Cancio, M. Pizzocaro, D. Calonico, F. Levi, *et al.*, arXiv:1406.6642.
  - [81] F. Scazza, C. Hofrichter, M. Höfer, P. De Groot, I. Bloch, and S. Fölling, arXiv:1403.4761.
  - [82] M. Lahrz, M. Lemesko, K. Sengstock, C. Becker, and L. Mathey, Phys. Rev. A **89**, 043616 (2014).
  - [83] P. O. Fedichev, Y. Kagan, G. V. Shlyapnikov, and J. Walraven, Phys. Rev. Lett. **77**, 2913 (1996).
  - [84] M. Theis, G. Thalhammer, K. Winkler, M. Hellwig, G. Ruff, R. Grimm, and J. H. Denschlag, Phys. Rev. Lett. **93**, 123001 (2004).
  - [85] K. Goyal, I. Reichenbach, and I. Deutsch, Phys. Rev. A **82**, 062704 (2010).
  - [86] R. A. Williams, L. J. LeBlanc, K. Jimenez-Garcia, M. C. Beeler, A. R. Perry, W. D. Phillips, and I. B. Spielman, Science **335**, 314 (2012).
  - [87] P. Wang, Z.-Q. Yu, Z. Fu, J. Miao, L. Huang, S. Chai, H. Zhai, and J. Zhang, Phys. Rev. Lett. **109**, 095301 (2012).
  - [88] R. A. Williams, M. C. Beeler, L. J. LeBlanc, K. Jiménez-García, and I. Spielman, Phys. Rev. Lett. **111**, 095301 (2013).
  - [89] I. Bloch, J. Dalibard, and W. Zwerger, Rev. Mod. Phys. **80**, 885 (2008).